Control of the temperature signal in Antarctic proxies by snowfall dynamics

Aymeric P. M. Servettaz[1], Cécile Agosta[2], Christoph Kittel[3, 4], and Anaïs J. Orsi[5]

[1]Biogeochemistry Research Center, Japan Agency for Marine-Earth Science and Technology, Yokosuka, 237-0061, Japan
5 [2]Laboratoire des Sciences du Climat et de l'Environnement, LSCE/IPSL, CEA-CNRS-UVSQ, Université Paris-Saclay, Gif-sur-Yvette, 91190, France
[3]Department of Geography, UR SPHERES, University of Liège, Liège, Belgium
[4]Institut des Géosciences de l'Environnement, University Grenoble Alpes/CNRS/IRD/G-INP, Grenoble, 38000, France
[5]Department of Earth, Ocean and Atmospheric Sciences, University of British Columbia, Vancouver, V6T 1Z4, British
10 Columbia, Canada

Correspondence to: Aymeric P. M. Servettaz (servettaza@jamstec.go.jp)

Abstract. Antarctica, the coldest and driest continent, is home to the largest ice sheet, whose mass is predominantly recharged by snowfall. A common feature of polar regions is the warming associated with snowfall, as moist oceanic air and cloud cover

15   increase the surface temperature. Consequently, snow accumulated onto the ice sheet is deposited under unusually warm conditions. Here we use a polar-oriented regional atmospheric model to study the statistical difference between average and snowfall-weighted temperatures. During snowfall, the warm anomaly scales with snowfall amount, with strongest sensitivity at low accumulation sites. Heavier snowfall in winter contributes to cool the annual snowfall-weighted temperature, but this effect is overwritten by the event-scale warming associated with precipitating atmospheric systems, which particularly contrast

20   with the extremely cold conditions in winter. Consequently, the seasonal range of snowfall-weighted temperature is reduced by 20 %. On the other hand, annual snowfall-weighted temperature shows 80 % more interannual variability than annual temperature, due to irregularity of snowfall occurrence and their associated temperature anomaly. Disturbance in apparent annual temperature cycle and interannual variability have important consequences for the interpretation of water isotopes in precipitation, which are deposited with snowfall and commonly used for paleo-temperature reconstructions from ice cores.

25   **Highlights**

- Snow precipitation events in Antarctica are associated with warm surface temperature anomalies that scale with snowfall rates.
- Snowfall-weighted climate normal temperature has a seasonal amplitude reduced by 20 %
- Annually snowfall-weighted temperature shows 80 % more interannual variability than annual temperature.

30   - Water isotopes reflect snowfall-weighted temperature and may be affected by such biases.

1 Introduction

Knowledge of temperature variability in Antarctica strongly relies on paleoclimate studies to extend the time period beyond the observation period of the satellite era (Jones et al., 2016). Of the temperature proxies, water stable isotopes in ice are the most used in paleoclimate studies in Antarctica (Stenni et al., 2017), due to the widely available base material and a good

35   understanding of the fractionation processes associated with precipitation formation (Markle and Steig, 2022). However, the relationship between average temperature at a location and isotopes in the snow is altered by deposition dynamics of snowfall-born water isotopes (Werner et al., 2000; Persson et al., 2011; Casado et al., 2020), and post-deposition processes such as ablation-redeposition and sublimation-condensation cycles (Steen-Larsen et al., 2014; Touzeau et al., 2016; Stenni et al., 2016; Münch et al., 2017; Hughes et al., 2021). Water isotope measurements characterize ice deposited during snowfall events,

40   therefore $\delta^{18}O$ (following the δ notation as in Dansgaard, 1964) is thought to better correlate with snowfall-weighted temperature than average temperature (Stenni et al., 2016; Fujita and Abe, 2006), as shown in isotope-enabled models (Sturm

et al., 2010). Differences between the snowfall-weighted temperature and average temperature remain poorly described, and characterizing these differences will help understand the signal recorded in water isotopes.

Precipitating atmospheric systems in polar regions are known to warm the surface temperature (Uotila et al., 2011). This is

45 caused by atmospheric perturbations and clouds strongly disturbing the surface energy balance: while short-wave radiation is reduced during overcast weather, absorption of snow-emitted long-wave radiation and downward radiation from the cloud base cause the net radiative heat flux to warm the surface (Nardino and Georgiadis, 2003; Van Den Broeke et al., 2006). Snow accumulated onto the Antarctic ice sheet is mostly deposited under cloudy conditions, except for the higher parts of Antarctic Plateau where clear-sky precipitations form a large part of the total ice accumulation (Stenni et al., 2016; Fujita and Abe, 2006;

50 Bromwich, 1988). Even for clear-sky precipitations, despite the absence of clouds, a vapor-rich atmosphere emits stronger long-wave radiation and warms the surface (Gallée and Gorodetskaya, 2010; Genthon et al., 2013). Atmospheric perturbations can increase surface wind-speed (Argentini et al., 2014; Vignon et al., 2017; Baas et al., 2019). This weakens or breaks the surface temperature inversion, due to increased turbulent mixing incorporating hot air from the upper temperature inversion layer (Hirasawa et al., 2000; Vignon et al., 2019; Heinemann et al., 2019). In addition to modification of the local energy

55 balance, synoptic systems effectively transport heat inland Antarctica (Carleton and Whalley, 1988; Giovinetto et al., 1992). Large atmospheric perturbations thus modify heat flux and surface temperature (Uotila et al., 2011), causing occasional surface warming exceeding 10°C (Ganeshan et al., 2022). Atmospheric rivers, which are extreme water vapor fluxes associated with some cyclones, are also associated with intense warming, particularly in winter (Wille et al., 2021). Consequently, days with snow or ice accumulation in Antarctica are warmer than average.

60 In Antarctica, a few large precipitation events can cause most of the inter-annual accumulation amount and variability (Turner et al., 2019). Consequently, these events control the temperature signal imprinted in the deposited snow isotopic composition. The few days when most of the snow is accumulated may not represent average conditions, because they are associated with warming, and may occur anytime in the year, causing aliasing of the seasonal signal by irregular sampling. Quantifying the temperature changes associated with snowfall could highlight key mechanisms for interpretation of water isotopes in snow and

65 ice, and ultimately improve water-isotope-based temperature reconstructions. Although the different heat transport mechanisms are relatively well understood and included in current atmospheric models, a climatology of the warming associated with snowfall events has not been made so far.

Here, we study the surface temperature changes associated with snowfall, aiming to understand the signal that a precipitation-based proxy would carry at time of its deposition. Using the polar-oriented regional atmospheric model MAR, extensively

70 evaluated for its representation of Antarctic surface mass balance (Agosta et al., 2019) and temperature (Kittel et al., 2021), we compute snowfall-weighted statistics to evaluate the average bias and interannual variability of temperature across Antarctica for the period 1979–2020. We focus our analysis on the quantification of temperature anomaly, defined as the difference to the daily climate normal temperature, and suggest possible effects on water isotopes.

2 Methods

2.1 Regional Atmospheric Model

We use the polar oriented regional atmospheric model MAR, in its version MARv 3.12 to assess the variability of snowfall and temperature in Antarctica. This model has shown good performance in its version 3.11 to represent the surface mass balance (defined as difference of total precipitation minus evaporation and runoff, Agosta et al., 2019), temperature (Kittel et al., 2021) and cloud (Kittel et al., 2022) variability. The version 3.12 used here differs mainly in the temperature transition of rainfall to snowfall where both can now co-occur in the model, and a correction of snowpack temperature (Antwerpen et al., 2022) as well as albedo tuning for the dense Antarctic snow. The simulation domain is on an Antarctic polar stereographic projection (EPSG:3031), with horizontal resolution of 35×35 km. The MAR model is nudged to ERA5, the latest re-analysis product of the European Center for Medium-Range Weather Forecast, with the most accurate representation of both temperature and surface mass balance in Antarctica among climate re-analyses (Gossart et al., 2019). The use of the MAR regional model enables further detail in the near-surface atmospheric layers and spatial scale compared to ERA5. The simulation used in this study covers the 1979–2020 period (42 years). There is a notable lack of direct snowfall observations in the low-accumulation regions of Antarctica, which hinders our ability to directly evaluate the model on this parameter. Modelled surface mass balance can be evaluated against observed accumulation, but includes several processes from snowfall to snow drift, evaporation of falling snow, and evaporation-condensation on the snow surface, which each come with their uncertainties. We evaluate the performance of MARv3.12 to represent temperature and surface mass balance in Figs. A1–A3.

2.2 Temperature averaging, difference, anomaly definitions and notations

We chose to use surface air temperature at 2-m for simplicity, because condensation levels change both spatially and temporally. If we used the condensation-level temperature, the difference with climate normal would depend on the level of precipitation formation, and may be vertically spread on the atmospheric column, making the comparison more complex. Choosing the surface temperature also enables comparison with available observations, and this is the level also considered in many paleotemperature reconstructions.

In this study, we use average temperature, calculated with the arithmetic mean:

$$T = \frac{\sum_{day=1}^{n_{days}} T_{day}}{n_{days}} \qquad (1)$$

and snowfall-weighted temperatures, defined as the weighted average of temperature with daily snowfall rate as the weighting coefficient:

$$T_w = \frac{\sum_{day=1}^{n_{days}} T_{day} \times SF_{day}}{\sum_{day=1}^{n_{days}} SF_{day}} \qquad (2)$$

In both cases, T_{day} refers to the temperature on a given day, and SF_{day} is the snowfall on the same day. Temperature averages can be computed for the entire study period (n_{days} = 15341), a year (n_{days} = 366), or on a given day of year (n_{days} = 42, used for climate normals $\bar{T}$ and $\overline{T_w}$). We define the climate normal temperature for each model grid cell as the average on the same day of year for the 42 years, and subsequently apply a 30-day rolling mean to smooth the signal.

We define the snowfall-weighted temperature difference as:

$$\Delta T = T_w - T \tag{3}$$

Decomposition of daily temperature T_{day} into climate normal temperature on that day ($\bar{T}_{day}$) and daily anomaly to climate normal (T'_{day}) allows us to separate the seasonal and non-seasonal effects of snowfall weighting.

$$\Delta T = \frac{\sum_{day=1}^{n_{days}}\left(\bar{T}_{day} + T'_{day}\right) \times SF_{day}}{\sum_{day=1}^{n_{days}} SF_{day}} - \frac{\sum_{day=1}^{n_{days}}\left(\bar{T}_{day} + T'_{day}\right)}{n_{days}} \tag{4}$$

$$\Delta T = \underbrace{\frac{\sum_{day=1}^{n_{days}}\bar{T}_{day} \times SF_{day}}{\sum_{day=1}^{n_{days}} SF_{day}} - \frac{\sum_{day=1}^{n_{days}}\bar{T}_{day}}{n_{days}}}_{seasonal} + \underbrace{\frac{\sum_{day=1}^{n_{days}}T'_{day} \times SF_{day}}{\sum_{day=1}^{n_{days}} SF_{day}} - \underbrace{\frac{\sum_{day=1}^{n_{days}}T'_{day}}{n_{days}}}_{= 0}}_{non-seasonal} \tag{5}$$

A summary of abbreviations used is given in Table 1.

3 Results and discussion

3.1 Average temperature during snowfall

The temperature during snowfall is statistically warmer than average temperature on the same day, as shown by the mostly positive temperature anomalies (Fig. 1). Despite a wide distribution of temperature anomalies at any given snowfall rate, the temperature anomaly increases with snowfall. Over Antarctica, there is a +5°C increase between snowfall rates of 0 (no snowfall) to 1 kg m^{-2} day^{-1}, and a gradual increase of another +5°C as snowfall rates increase from 1 up to 100 kg m^{-2} day^{-1}. Conversely, days without snowfall are 2°C cooler than average. For major regions of Antarctica, similar patterns are observed with negative temperature anomalies on days without snowfall, and increasing temperature anomalies, up to +10°C for snowfall exceeding 50 kg m^{-2} day^{-1}. The main difference for East Antarctic high elevations (Fig. 1f) is that the temperature anomalies reach the +5°C threshold for snowfall rates of less than 1 kg m^{-2} day^{-1}.

The warm anomaly associated with snowfall affects all the Antarctic continent although with varying intensity as shown by the map of differences between snowfall-weighted temperature and average temperature (noted ΔT, Fig. 2, abbreviations listed in Table 1). Over the entire Antarctic continent and ice shelves, ΔT averages 5.4°C. While coastal regions and West Antarctica show ΔT of 0 to 5°C, the East Antarctic Plateau and ice shelves reach ΔT of up to 10°C. Interestingly, ΔT is the highest in large topographical depressions such as in the Recovery (20° W, 80° S), Aurora (115° E, 75° S) and Wilkes (150° E, 70° S) basins, or the Byrd glacier catchment inland of transantarctic mountains (150° E, 80° S). On the other hand, over steep slopes and

130   ridges, snowfall-weighted temperature is relatively closer to average temperature. Note that hoar frost is computed separately
from snowfall in the model, and occurs in cold conditions (Schlosser et al., 2016). Therefore, ice accumulated by hoar frost
can mitigate the warm conditions associated with snowfall, but this is not depicted by ΔT that accounts only for snowfall.

To better understand the temperature anomaly associated with snowfall at the Antarctic scale, we analyse 10 sites where the
impact of extreme precipitation events on total accumulation has previously been discussed (Turner et al., 2019), and show the

135   temperature−snowfall relationship at these locations (inserts in Fig. 2). There are strong differences between sites located near
the coast (Law Dome, East and West Peninsula, Gomez) compared to high elevation sites on the East Antarctic Plateau (High
Plateau, Dronning Maud Land, Dome C): high elevation sites are characterized by low snowfall rates, but events causing
snowfall larger than 1 kg m^{-2} d^{-1} are accompanied by a warming of more than 10°C on average, and commonly up to 20°C
(Table 2). These high elevation sites with low snowfall and large temperature anomalies are responsible for the sharp increase

140   in temperature associated with low snowfall rates (Fig. 1f). Most locations reach temperature anomalies close to 10°C at their
respective maximum snowfall (WAIS Divide, Gomez, Law Dome), except for sites where dry warming usually occurs, driven
by Foehn (East Peninsula) or katabatic adiabatic compression (coastal slopes). Each site shows a warming trend with increasing
snowfall rate, with greater warming trends for sites with low accumulation (Fig. 2). Overall, days with snowfall are statistically
warmer than average conditions, and increasingly so for higher snowfall rates at a given location.

145   **3.2 Variability of temperature during snowfall**

Snowfall events, in particular large precipitation events, are an important source of variability in the Antarctic climate (Turner
et al., 2019). As there is a clear link between snowfall intensity and temperature anomaly, the variability of snowfall translates
to the variability of temperature. We first investigate the seasonality of temperature anomalies associated with snowfall (Fig.
3), by considering the climate normal snowfall-weighted temperature ($\overline{T_w}$, see Sect. 2 Methods for details on computation) and

150   the climate normal temperature ($\overline{T}$). $\overline{T_w}$ differs from $\overline{T}$ by 3°C in summer, and up to 8°C in winter on average on the Antarctic
ice sheet. The larger difference in winter emerges from the strong warming associated with precipitating atmospheric systems
that particularly stand out from the usual cold dry conditions. Indeed, the $\overline{T}$ reaches extremely low temperatures in winter,
driven by the strong surface radiative cooling (Connolley, 1996; Hudson and Brandt, 2005; Genthon et al., 2021). While it
contributes to large variability in winter temperatures compared to summer season (Ricaud et al., 2017), snowfall consistently

155   occurs under warm conditions. The seasonal amplitude of $\overline{T_w}$ is thus 20 % lower than that of $\overline{T}$ on average in Antarctica
(Fig. 4). Reduction of seasonal amplitude occurs consistently over the Antarctic continent, and is strongest in coastal slopes.
In winter, cyclogenesis is slightly higher (Uotila et al., 2011), and atmospheric blockings are more frequent (Wille et al., 2021;
Scarchilli et al., 2011), increasing the probability of poleward moisture transport and Antarctic snowfall. This results in higher
snowfall in the winter months at the Antarctic scale (Fig. 3b) and causes snowfall-weighted temperature to be influenced more

160   by the winter season, when the snowfall-related warming is the strongest. We decomposed the contributions of seasonal
distribution of snowfall (Fig. 5a) and event-related daily temperature anomaly (Fig. 5b) to ΔT. As most of Antarctica receives
more snowfall in winter (Palerme et al., 2017), the difference induced by seasonality averages −0.7°C over the ice sheet, but

rarely exceeds −3°C. On the contrary, snowfall event-related warming causes a difference of +6.1°C, and dominates the difference between snowfall-weighted and all-day temperatures.

165   The dampened seasonal amplitude of snowfall-weighted temperature results from averaging 42 years, smoothing out interannual variability. While annually averaged temperature is relatively stable through time (Fig. 6a), interannual snowfall is highly variable, especially for the winter season (Casado et al., 2020; Turner et al., 2019). It causes the annual snowfall-weighted temperature to vary significantly from one year to another, with a standard deviation increased by +80 % on average over the ice sheet compared to annual-mean temperature (Fig. 6d). The variability is especially increased in Dronning Maud

170 Land and the Eastern part of West Antarctica, facing the Ronne Ice Shelf, where the interannual variability of snowfall-weighted temperature can be 200 % larger than interannual temperature variability. Previous studies highlighted that the large variability of winter temperatures causes the winter season to be dominant in the interannual temperature variability, as a warm year is usually due to a warm winter, often accompanied with one or multiple snowfall events in winter (Persson et al., 2011; Casado et al., 2020; Servettaz et al., 2020). Despite the reduced seasonality of snowfall-weighted temperature and the tendency

175 to oversample warm winters, its interannual variability is increased. In other words, the temperature averaged equally over all days of a year is more stable than the temperature taken during snowfall only, because of the sporadic nature of snowfall, which subsamples the temperature of a limited number of days (Fujita and Abe, 2006; Turner et al., 2019) at random times of the year, and with a temperature bias which depends on precipitation intensity. On the interannual scale, the variability of yearly averaged temperature is thus enhanced when weighting with snowfall.

180   **3.3 Implications for water isotopes**

Water isotopes are used in Antarctic paleoclimate studies as a proxy for temperature due to the relationship between air temperature at condensation and the isotopic ratio in precipitation (Stenni et al., 2017; Dansgaard, 1964). Ice cores retrieve material accumulated over time onto the ice sheet, where the ice mass contribution depends on the snowfall. Therefore, snowfall-weighted temperatures provide an analogue to the isotopes we can expect to measure in an ice core. We thus discuss

185 how temperature during snowfall may affect $\delta^{18}O$ at time of snow deposition, prior to post-deposition effects that occur later and further modify snow isotopes.

Water isotopes in snow are deposited under warmer-than-normal conditions (Fig. 2), which leads to higher-than-expected $\delta^{18}O$. Some climatic information is lost for $\delta^{18}O$ as cold days are not recorded, or recorded with lower weight. Previous works suggested that $\delta^{18}O$ could be seasonally biased due to the annual cycle of snowfall (Markle and Steig, 2022; Werner et al.,

190 2000; Persson et al., 2011), but here we showed that the warm bias associated with precipitation events is clearly the main factor controlling snowfall-weighted temperature in Antarctica. The variety of ΔT across modern Antarctica suggests that it depends on precipitation regimes and amplitude of temperature change during precipitation at a given site. The stability of ΔT through time is thus decisive for temperature reconstructions based on isotopes because temporal changes of ΔT could accompany temperature and precipitations changes, and hinder the $\delta^{18}O$-based reconstructions. Here the short study period

195 does not allow to evaluate temporal changes in ΔT, but such changes may be responsible for modifications of $\delta^{18}O$–temperature

slopes at longer timescales, as was suggested for the glacial-interglacial range (Buizert et al., 2021). Moreover, the reduced annual cycle of $\overline{T_w}$ relative to $\overline{T}$ may reflect a lower annual cycle of $\delta^{18}O$, which can explain why seasonal $\delta^{18}O$-temperature slope appears lower in precipitation $\delta^{18}O$ studies than in simple isotopic models (Casado et al., 2018). On the other hand, averaging temperature and isotopes yearly to define the $\delta^{18}O$-temperature slope may increase the slope value because of the

200   higher interannual variability of $\delta^{18}O$ induced by irregularity of the snowfall distribution, similarly to snowfall-weighted temperature.

Slopes of snowfall-weighted $\delta^{18}O$ against snowfall-weighted temperature have been previously suggested (Fujita and Abe, 2006; Sturm et al., 2010; Servettaz et al., 2020). Precipitation-weighted $\delta^{18}O$ makes physical sense because it mimics ice core signal — omitting the post-deposition effects —, but paleo-climate reconstructions seek temperature rather than snowfall-

205   weighted temperature. This work highlights the critical importance of event-related warming on the temperature during snowfall, which reduces seasonal amplitude, while irregular snowfall distribution enhances interannual variability of the temperature possibly recorded in water isotopes. Understanding the effect of snowfall weighting on temperature average at ice coring sites will help reconstruct paleo-temperature more accurately, and future efforts should account for the difference in temperature between condensation level and surface, often dictated by inversion strength. Depending on the targeted time

210   frame for temperature reconstruction from isotopes, be it seasonal (Jones et al., 2023) or pluriannual (Stenni et al., 2017), the reconstructed temperature range may be lessened or increased. Quantifying the local effect of snowfall-weighting on temperature range can help refine the temperature-isotope slopes for a more accurate estimation. Greater snowfall-weighted temperature differences at low-accumulation sites suggest that changes in snowfall regimes could impact the temperature difference, and thus bias the reconstructions from isotopes. Further work is necessary to fully understand how change in

215   snowfall dynamics may influence temperature reconstructions from isotopes, which may be facilitated by atmospheric models equipped with isotopes.

4 Conclusions

We evaluated the temperature during snowfall in Antarctica using the regional atmospheric climate model MAR. Warm temperature anomalies usually accompany snowfalls, and the anomalies tend to increase with snowfall rate at any given site.

220   The trend of temperature increase is strongest at sites with low accumulation, so that even locations with low snowfall rates experience a strong snowfall-weighted temperature difference. Over the Antarctic continent, this difference averages 5.4°C. Temperature anomalies are typically strongest in winter, which leads to a 20 % reduced amplitude in the seasonal cycle of snowfall-weighted climate normal temperature. Larger temperature anomalies during winter also offset the slightly higher seasonal contribution of winter precipitations which would reduce the snowfall-weighted temperature by 0.7°C. Year to year

225   irregularities in snowfall distribution contribute to randomly subsample temperature, and increase interannual variability of snowfall-weighted temperature, making it 80 % more variable. Under the assumption that water isotopes reflect snowfall-weighted temperature, these biases will transfer to the isotopic signal in ice cores, which may explain the necessity to adjust

isotope-temperature slope values depending on the timeframe of the reconstruction. While we focused on the 1979–2020 period in this study, potential changes in precipitation regimes at longer timescales may be associated with changes in the

230 snowfall-weighted biases, and deserve attention in future studies to adjust the isotope-temperature slopes accordingly for quantitatively accurate paleo-temperature reconstructions.

Appendix A Evaluation of MAR performance

(Figures only)

Code availability

235 The code for the regional atmospheric climate model MAR (Modèle Atmosphérique Régional) is available upon registration at https://gitlab.com/Mar-Group/MARv3 [last access: August 2023]. Python code for computations and figure creation is available at https://gitlab.com/aymericservettaz/antarctic-temperature-anomalies [last updated: August 2023].

Data availability

The MAR simulation used in this study is available upon request to the corresponding author.

240 **Author contribution**

CA and CK participated in the development of the MAR model and its application in the Antarctic region. AS designed the study, performed formal analysis of model outputs, and wrote the initial draft. AS and CA created figures. AO provided ideas and guidance for the manuscript composition. All authors contributed to writing and editing the manuscript.

Competing interests

245 The authors declare that they have no conflict of interest.

References

Agosta, C., Amory, C., Kittel, C., Orsi, A. J., Favier, V., Gallée, H., van den Broeke, M. R., Lenaerts, J. T. M., van Wessem, J. M., van de Berg, W. J., and Fettweis, X.: Estimation of the Antarctic surface mass balance using the regional climate model MAR (1979–2015) and identification of dominant processes, The Cryosphere, 13, 281–296, https://doi.org/10.5194/tc-13-281-2019, 2019.

Antwerpen, R. M., Tedesco, M., Fettweis, X., Alexander, P., and van de Berg, W. J.: Assessing bare-ice albedo simulated by MAR over the Greenland ice sheet (2000–2021) and implications for meltwater production estimates, The Cryosphere, 16, 4185–4199, https://doi.org/10.5194/tc-16-4185-2022, 2022.

255 Argentini, S., Pietroni, I., Mastrantonio, G., Viola, A. P., Dargaud, G., and Petenko, I.: Observations of near surface wind speed, temperature and radiative budget at Dome C, Antarctic Plateau during 2005, Antarctic Science, 26, 104–112, https://doi.org/10.1017/S0954102013000382, 2014.

Baas, P., van de Wiel, B. J. H., van Meijgaard, E., Vignon, E., Genthon, C., van der Linden, S. J. A., and de Roode, S. R.: Transitions in the wintertime near-surface temperature inversion at Dome C, Antarctica, Quarterly Journal of the Royal Meteorological Society, 145, 930–946, https://doi.org/10.1002/qj.3450, 2019.

260 Bromwich, D. H.: Snowfall in high southern latitudes, Reviews of Geophysics, 26, 149–168, https://doi.org/10.1029/RG026i001p00149, 1988.

Buizert, C., Fudge, T. J., Roberts, W. H. G., Steig, E. J., Sherriff-Tadano, S., Ritz, C., Lefebvre, E., Edwards, J., Kawamura, K., Oyabu, I., Motoyama, H., Kahle, E. C., Jones, T. R., Abe-Ouchi, A., Obase, T., Martin, C., Corr, H., Severinghaus, J. P., Beaudette, R., Epifanio, J. A., Brook, E. J., Martin, K., Chappellaz, J., Aoki, S., Nakazawa, T., Sowers, T. A., Alley, R. B., 265 Ahn, J., Sigl, M., Severi, M., Dunbar, N. W., Svensson, A., Fegyveresi, J. M., He, C., Liu, Z., Zhu, J., Otto-Bliesner, B. L., Lipenkov, V. Y., Kageyama, M., and Schwander, J.: Antarctic surface temperature and elevation during the Last Glacial Maximum, Science, 372, 1097–1101, https://doi.org/10.1126/science.abd2897, 2021.

Carleton, A. M. and Whalley, D.: Eddy transport of sensible heat and the life history of synoptic systems: A statistical analysis for the Southern Hemisphere winter, Meteorl. Atmos. Phys., 38, 140–152, https://doi.org/10.1007/BF01029778, 1988.

270 Casado, M., Landais, A., Picard, G., Münch, T., Laepple, T., Stenni, B., Dreossi, G., Ekaykin, A., Arnaud, L., Genthon, C., Touzeau, A., Masson-Delmotte, V., and Jouzel, J.: Archival processes of the water stable isotope signal in East Antarctic ice cores, The Cryosphere, 12, 1745–1766, https://doi.org/10.5194/tc-12-1745-2018, 2018.

Casado, M., Münch, T., and Laepple, T.: Climatic information archived in ice cores: impact of intermittency and diffusion on the recorded isotopic signal in Antarctica, Clim. Past, 16, 1581–1598, https://doi.org/10.5194/cp-16-1581-2020, 2020.

275 Connolley, W. M.: The Antarctic Temperature Inversion, International Journal of Climatology, 16, 1333–1342, https://doi.org/10.1002/(SICI)1097-0088(199612)16:12<1333::AID-JOC96>3.0.CO;2-6, 1996.

Dansgaard, W.: Stable isotopes in precipitation, Tellus, 16, 436–468, https://doi.org/10.1111/j.2153-3490.1964.tb00181.x, 1964.

Fujita, K. and Abe, O.: Stable isotopes in daily precipitation at Dome Fuji, East Antarctica, Geophysical Research Letters, 33, 280 article L18503, https://doi.org/10.1029/2006GL026936, 2006.

Gallée, H. and Gorodetskaya, I. V.: Validation of a limited area model over Dome C, Antarctic Plateau, during winter, Clim Dyn, 34, 61–72, https://doi.org/10.1007/s00382-008-0499-y, 2010.

Ganeshan, M., Yang, Y., and Palm, Stephen. P.: Impact of Clouds and Blowing Snow on Surface and Atmospheric Boundary Layer Properties Over Dome C, Antarctica, Journal of Geophysical Research: Atmospheres, 127, e2022JD036801, 285 https://doi.org/10.1029/2022JD036801, 2022.

Genthon, C., Six, D., Gallée, H., Grigioni, P., and Pellegrini, A.: Two years of atmospheric boundary layer observations on a 45-m tower at Dome C on the Antarctic plateau, Journal of Geophysical Research: Atmospheres, 118, 3218–3232, https://doi.org/10.1002/jgrd.50128, 2013.

290 Genthon, C., Veron, D., Vignon, E., Six, D., Dufresne, J.-L., Madeleine, J.-B., Sultan, E., and Forget, F.: 10 years of temperature and wind observation on a 45 m tower at Dome C, East Antarctic plateau, Earth System Science Data, 13, 5731–5746, https://doi.org/10.5194/essd-13-5731-2021, 2021.

Giovinetto, M. B., Bromwich, D. H., and Wendler, G.: Atmospheric net transport of water vapor and latent heat across 70°S, Journal of Geophysical Research: Atmospheres, 97, 917–930, https://doi.org/10.1029/91JD02485, 1992.

Gossart, A., Helsen, S., Lenaerts, J. T. M., Broucke, S. V., van Lipzig, N. P. M., and Souverijns, N.: An Evaluation of Surface
295 Climatology in State-of-the-Art Reanalyses over the Antarctic Ice Sheet, Journal of Climate, 32, 6899–6915, https://doi.org/10.1175/JCLI-D-19-0030.1, 2019.

Heinemann, G., Glaw, L., and Willmes, S.: A Satellite-Based Climatology of Wind-Induced Surface Temperature Anomalies for the Antarctic, Remote Sensing, 11, 1539, https://doi.org/10.3390/rs11131539, 2019.

Hirasawa, N., Nakamura, H., and Yamanouchi, T.: Abrupt changes in meteorological conditions observed at an inland
300 Antarctic Station in association with wintertime blocking, Geophysical Research Letters, 27, 1911–1914, https://doi.org/10.1029/1999GL011039, 2000.

Hudson, S. R. and Brandt, R. E.: A Look at the Surface-Based Temperature Inversion on the Antarctic Plateau, Journal of Climate, 18, 1673–1696, https://doi.org/10.1175/JCLI3360.1, 2005.

Hughes, A. G., Wahl, S., Jones, T. R., Zuhr, A., Hörhold, M., White, J. W. C., and Steen-Larsen, H. C.: The role of sublimation
305 as a driver of climate signals in the water isotope content of surface snow: laboratory and field experimental results, The Cryosphere, 15, 4949–4974, https://doi.org/10.5194/tc-15-4949-2021, 2021.

Jones, J. M., Gille, S. T., Goosse, H., Abram, N. J., Canziani, P. O., Charman, D. J., Clem, K. R., Crosta, X., de Lavergne, C., Eisenman, I., England, M. H., Fogt, R. L., Frankcombe, L. M., Marshall, G. J., Masson-Delmotte, V., Morrison, A. K., Orsi, A. J., Raphael, M. N., Renwick, J. A., Schneider, D. P., Simpkins, G. R., Steig, E. J., Stenni, B., Swingedouw, D., and Vance,
310 T. R.: Assessing recent trends in high-latitude Southern Hemisphere surface climate, Nature Clim Change, 6, 917–926, https://doi.org/10.1038/nclimate3103, 2016.

Jones, T. R., Cuffey, K. M., Roberts, W. H. G., Markle, B. R., Steig, E. J., Stevens, C. M., Valdes, P. J., Fudge, T. J., Sigl, M., Hughes, A. G., Morris, V., Vaughn, B. H., Garland, J., Vinther, B. M., Rozmiarek, K. S., Brashear, C. A., and White, J. W. C.: Seasonal temperatures in West Antarctica during the Holocene, Nature, 613, 292–297, https://doi.org/10.1038/s41586-
315 022-05411-8, 2023.

Kittel, C., Amory, C., Agosta, C., Jourdain, N. C., Hofer, S., Delhasse, A., Doutreloup, S., Huot, P.-V., Lang, C., Fichefet, T., and Fettweis, X.: Diverging future surface mass balance between the Antarctic ice shelves and grounded ice sheet, The Cryosphere, 15, 1215–1236, https://doi.org/10.5194/tc-15-1215-2021, 2021.

Kittel, C., Amory, C., Hofer, S., Agosta, C., Jourdain, N. C., Gilbert, E., Le Toumelin, L., Vignon, É., Gallée, H., and Fettweis,
320 X.: Clouds drive differences in future surface melt over the Antarctic ice shelves, The Cryosphere, 16, 2655–2669, https://doi.org/10.5194/tc-16-2655-2022, 2022.

Markle, B. R. and Steig, E. J.: Improving temperature reconstructions from ice-core water-isotope records, Clim. Past, 18, 1321–1368, https://doi.org/10.5194/cp-18-1321-2022, 2022.

Mottram, R., Hansen, N., Kittel, C., van Wessem, J. M., Agosta, C., Amory, C., Boberg, F., van de Berg, W. J., Fettweis, X.,
325 Gossart, A., van Lipzig, N. P. M., van Meijgaard, E., Orr, A., Phillips, T., Webster, S., Simonsen, S. B., and Souverijns, N.:
What is the surface mass balance of Antarctica? An intercomparison of regional climate model estimates, The Cryosphere, 15,
3751–3784, https://doi.org/10.5194/tc-15-3751-2021, 2021.

Münch, T., Kipfstuhl, S., Freitag, J., Meyer, H., and Laepple, T.: Constraints on post-depositional isotope modifications in
East Antarctic firn from analysing temporal changes of isotope profiles, The Cryosphere, 11, 2175–2188,
330 https://doi.org/10.5194/tc-11-2175-2017, 2017.

Nardino, M. and Georgiadis, T.: Cloud type and cloud cover effects on the surface radiative balance at several Polar sites,
Theor. Appl. Climatol., 74, 203–215, https://doi.org/10.1007/s00704-002-0708-2, 2003.

Palerme, C., Claud, C., Dufour, A., Genthon, C., Wood, N. B., and L'Ecuyer, T.: Evaluation of Antarctic snowfall in global
meteorological reanalyses, Atmospheric Research, 190, 104–112, https://doi.org/10.1016/j.atmosres.2017.02.015, 2017.

335 Persson, A., Langen, P. L., Ditlevsen, P., and Vinther, B. M.: The influence of precipitation weighting on interannual variability
of stable water isotopes in Greenland, J. Geophys. Res., 116, D20120, https://doi.org/10.1029/2010JD015517, 2011.

Ricaud, P., Bazile, E., del Guasta, M., Lanconelli, C., Grigioni, P., and Mahjoub, A.: Genesis of diamond dust, ice fog and
thick cloud episodes observed and modelled above Dome C, Antarctica, Atmospheric Chemistry and Physics, 17, 5221–5237,
https://doi.org/10.5194/acp-17-5221-2017, 2017.

340 Scarchilli, C., Frezzotti, M., and Ruti, P. M.: Snow precipitation at four ice core sites in East Antarctica: provenance,
seasonality and blocking factors, Clim Dyn, 37, 2107–2125, https://doi.org/10.1007/s00382-010-0946-4, 2011.

Schlosser, E., Stenni, B., Valt, M., Cagnati, A., Powers, J. G., Manning, K. W., Raphael, M., and Duda, M. G.: Precipitation
and synoptic regime in two extreme years 2009 and 2010 at Dome C, Antarctica – implications for ice core interpretation,
Atmos. Chem. Phys., 16, 4757–4770, https://doi.org/10.5194/acp-16-4757-2016, 2016.

345 Servettaz, A. P. M., Orsi, A. J., Curran, M. A. J., Moy, A. D., Landais, A., Agosta, C., Winton, V. H. L., Touzeau, A.,
McConnell, J. R., Werner, M., and Baroni, M.: Snowfall and Water Stable Isotope Variability in East Antarctica Controlled
by Warm Synoptic Events, J. Geophys. Res. Atmos., 125, e2020JD032863, https://doi.org/10.1029/2020JD032863, 2020.

Steen-Larsen, H. C., Masson-Delmotte, V., Hirabayashi, M., Winkler, R., Satow, K., Prié, F., Bayou, N., Brun, E., Cuffey, K.
M., Dahl-Jensen, D., Dumont, M., Guillevic, M., Kipfstuhl, S., Landais, A., Popp, T., Risi, C., Steffen, K., Stenni, B., and
350 Sveinbjörnsdottír, A. E.: What controls the isotopic composition of Greenland surface snow?, Climate of the Past, 10, 377–
392, https://doi.org/10.5194/CP-10-377-2014, 2014.

Stenni, B., Scarchilli, C., Masson-Delmotte, V., Schlosser, E., Ciardini, V., Dreossi, G., Grigioni, P., Bonazza, M., Cagnati,
A., Karlicek, D., Risi, C., Udisti, R., and Valt, M.: Three-year monitoring of stable isotopes of precipitation at Concordia
Station, East Antarctica, The Cryosphere, 10, 2415–2428, https://doi.org/10.5194/tc-10-2415-2016, 2016.

355 Stenni, B., Curran, M. A. J., Abram, N. J., Orsi, A. J., Goursaud, S., Masson-Delmotte, V., Neukom, R., Goosse, H., Divine,
D., van Ommen, T., Steig, E. J., Dixon, D. A., Thomas, E. R., Bertler, N. A. N., Isaksson, E., Ekaykin, A., Werner, M., and
Frezzotti, M.: Antarctic climate variability on regional and continental scales over the last 2000 years, Clim. Past, 13, 1609–
1634, https://doi.org/10.5194/cp-13-1609-2017, 2017.

Sturm, C., Zhang, Q., and Noone, D.: An introduction to stable water isotopes in climate models: benefits of forward proxy
360 modelling for paleoclimatology, Climate of the Past, 6, 115–129, https://doi.org/10.5194/cp-6-115-2010, 2010.

Touzeau, A., Landais, A., Stenni, B., Uemura, R., Fukui, K., Fujita, S., Guilbaud, S., Ekaykin, A., Casado, M., Barkan, E., Luz, B., Magand, O., Teste, G., Meur, E. L., Baroni, M., Savarino, J., Bourgeois, I., and Risi, C.: Acquisition of isotopic composition for surface snow in East Antarctica and the links to climatic parameters, The Cryosphere, 10, 837–852, https://doi.org/doi:10.5194/tc-10-837-2016, 2016.

365 Turner, J., Phillips, T., Thamban, M., Rahaman, W., Marshall, G. J., Wille, J. D., Favier, V., Winton, V. H. L., Thomas, E., Wang, Z., Broeke, M. van den, Hosking, J. S., and Lachlan-Cope, T.: The Dominant Role of Extreme Precipitation Events in Antarctic Snowfall Variability, Geophysical Research Letters, 46, 3502–3511, https://doi.org/10.1029/2018GL081517, 2019.

Uotila, P., Vihma, T., Pezza, A. B., Simmonds, I., Keay, K., and Lynch, A. H.: Relationships between Antarctic cyclones and surface conditions as derived from high-resolution numerical weather prediction data, Journal of Geophysical Research: 370 Atmospheres, 116, D07109, https://doi.org/10.1029/2010JD015358, 2011.

Van Den Broeke, M., Reijmer, C., Van As, D., and Boot, W.: Daily cycle of the surface energy balance in Antarctica and the influence of clouds, International Journal of Climatology, 26, 1587–1605, https://doi.org/10.1002/joc.1323, 2006.

Vignon, E., van de Wiel, B. J. H., van Hooijdonk, I. G. S., Genthon, C., van der Linden, S. J. A., van Hooft, J. A., Baas, P., Maurel, W., Traullé, O., and Casasanta, G.: Stable boundary-layer regimes at Dome C, Antarctica: observation and analysis, 375 Quarterly Journal of the Royal Meteorological Society, 143, 1241–1253, https://doi.org/10.1002/qj.2998, 2017.

Vignon, É., Traullé, O., and Berne, A.: On the fine vertical structure of the low troposphere over the coastal margins of East Antarctica, Atmospheric Chemistry and Physics, 19, 4659–4683, https://doi.org/10.5194/acp-19-4659-2019, 2019.

Wang, Y., Ding, M., van Wessem, J. M., Schlosser, E., Altnau, S., van den Broeke, M. R., Lenaerts, J. T. M., Thomas, E. R., Isaksson, E., Wang, J., and Sun, W.: A Comparison of Antarctic Ice Sheet Surface Mass Balance from Atmospheric Climate 380 Models and In Situ Observations, Journal of Climate, 29, 5317–5337, https://doi.org/10.1175/JCLI-D-15-0642.1, 2016.

Werner, M., Mikolajewicz, U., Heimann, M., and Hoffmann, G.: Borehole versus isotope temperatures on Greenland: Seasonality does matter, Geophysical Research Letters, 27, 723–726, https://doi.org/10.1029/1999GL006075, 2000.

Wille, J. D., Favier, V., Gorodetskaya, I. V., Agosta, C., Kittel, C., Beeman, J. C., Jourdain, N. C., Lenaerts, J. T. M., and Codron, F.: Antarctic Atmospheric River Climatology and Precipitation Impacts, Journal of Geophysical Research: 385 Atmospheres, 126, e2020JD033788, https://doi.org/10.1029/2020JD033788, 2021.

Tables

Table 1. Abbreviations used in this study.

Abbr.	Full Name	Mathematic Definition	number of values at each location
T_w	snowfall-weighted average temperature	$T_w = \frac{\sum_{day=1}^{n_{days}} T_{day} \times SF_{day}}{\sum_{day=1}^{n_{days}} SF_{day}}$, for the entire study period	1
T	average temperature	$T = \frac{\sum_{day=1}^{n_{days}} T_{day}}{n_{days}}$, for the entire study period	1
ΔT	snowfall-weighted temperature difference	$\Delta T = T_w - T$	1
$\overline{T_w}$	climate normal snowfall-weighted temperature	For each day of year, same as T_w then 30-day rolling average	366 (one per day of year)
$\overline{T}$	climate normal temperature	For each day of year, same as T then 30-day rolling average	366 (one per day of year)
T'	Daily temperature anomaly to climate normal	Daily difference to $\overline{T}$ on the corresponding day of year	One per day

390

Table 2. Values of temperature anomalies (T') for snowfall rates higher than 1 kg m^{-2} d^{-1}. Locations of sites are shown in Fig. 2. For each site, average (arithmetic) and quantiles for different percentages are shown.

T' (°C) for SF > 1 kg m^{-2} d^{-1}	Dronning Maud Land	High Plateau	Law Dome	Dome C	Ross Ice Shelf	Ocean	WAIS Divide	Gomez	West Peninsula	East Peninsula
average	13.6	23.2	4.1	20.3	10.3	3.7	7.2	2.9	1.3	1.5
q95	20.8	27.9	10.6	31.3	22.0	13.4	14.4	9.8	7.3	8.9
q84 (+1σ)	18.1	27.2	8.0	26.9	16.9	9.2	11.8	7.3	4.9	5.3
q50	13.7	25.2	3.9	19.9	9.3	2.6	7.1	2.9	1.3	1.2
q16 (-1σ)	8.9	19.1	0.5	12.8	4.2	-0.4	2.9	-1.1	-1.9	-2.1
q05	5.6	17.2	-1.8	10.2	1.6	-4.0	0.0	-4.3	-4.7	-4.4

395

15
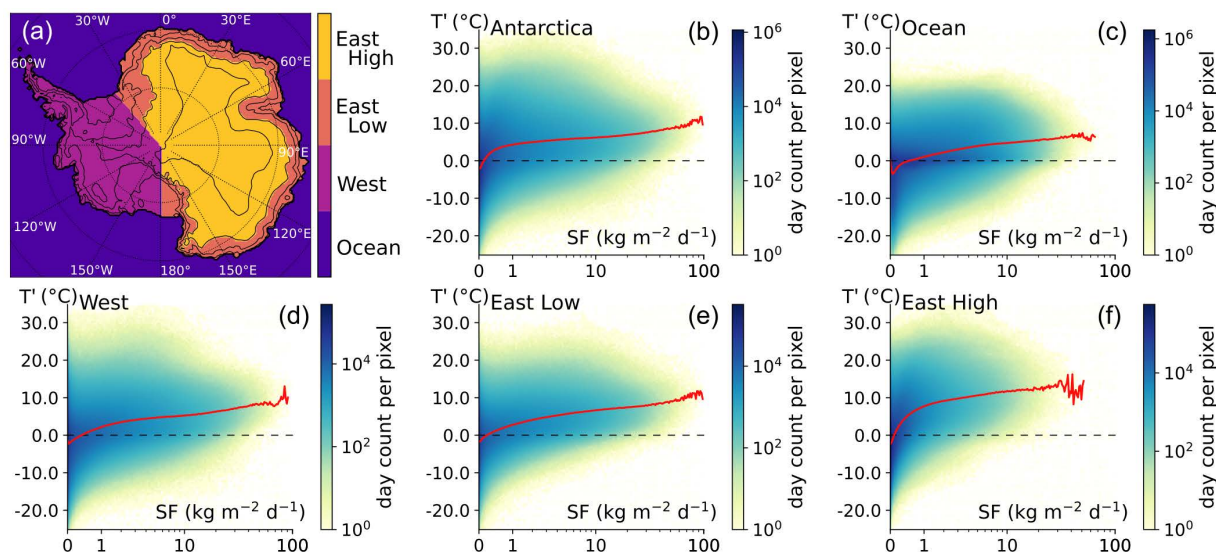
Figures

Figure 1. Scatter heatmaps of the daily temperature anomaly to climate normal as a function of daily snowfall, for different major regions of Antarctica, for the period 1979–2020. The temperature anomaly T' is defined as the difference between daily 2-m temperature and the climate normal $\bar{T}$ (temperature on the average seasonal cycle for this day, see Sect. 2 methods) on the corresponding model cell, for each day. Scatter heatmaps are represented for each region defined in (**a**), with Antarctica (**b**) regrouping every point on the surface of the Antarctic ice sheet (including ice shelves). Ocean (**c**) is the remaining model domain in the Southern Ocean. Antarctica is further subdivided in West (**d**) for longitudes between 180° W and 45° W, East Low (**e**) for longitudes between 45° W and 180° E and elevation below 2000 m and East High (**f**) for longitudes between 45° W and 180° E and elevation above 2000 m. For heatmaps (**b**–**f**), the red line represents the average temperature anomaly given the snowfall rate, dashed lines highlight the T'=0 (no anomaly), x-axis is linear with $\log_{10}(1+\text{snowfall})$, and scatter density was counted as the number of days in each pixel-sized bin after projection on the logarithmic snowfall scale.
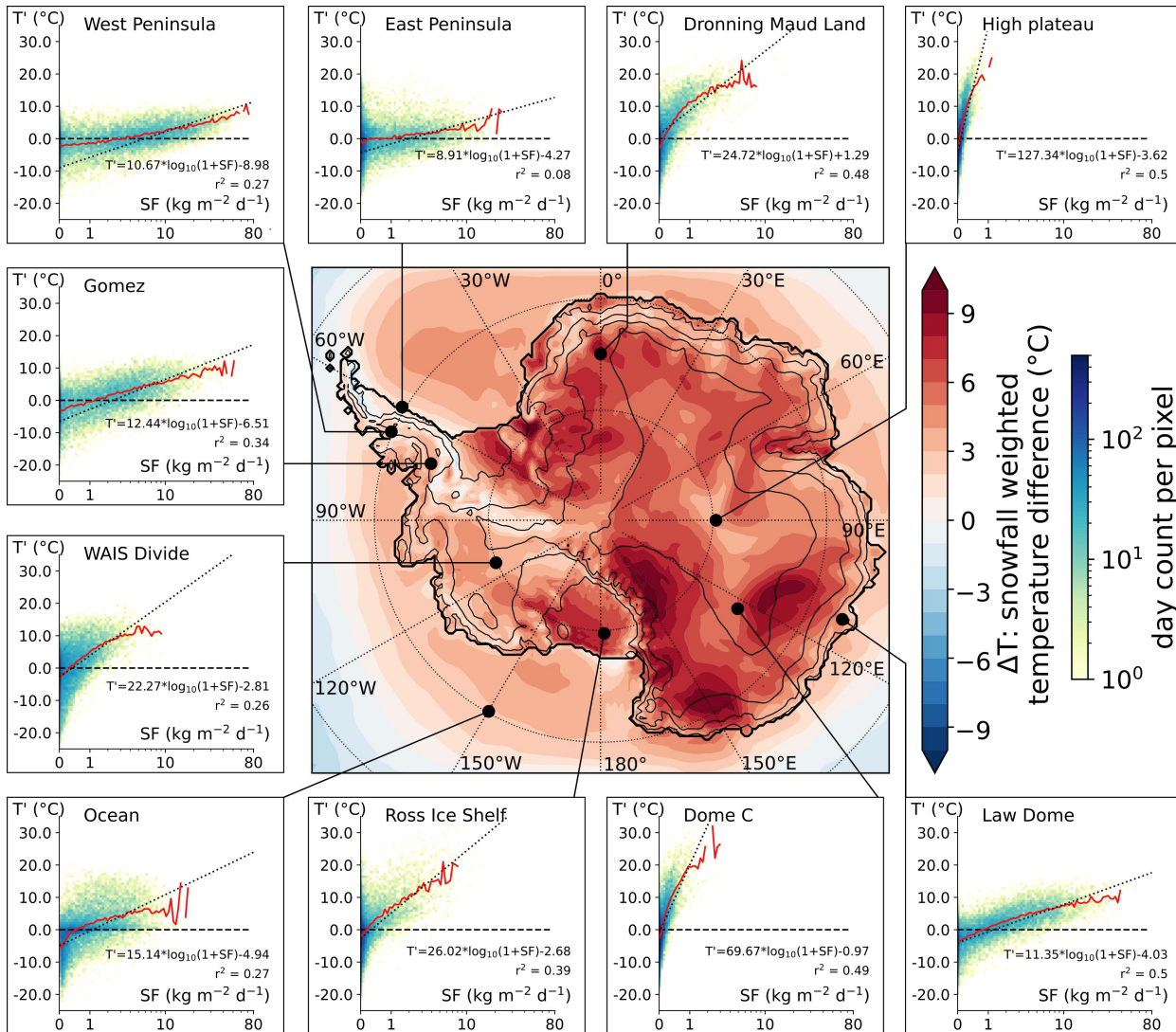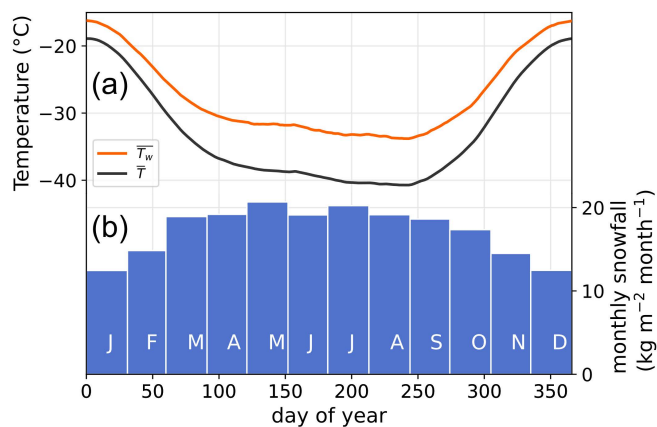
Figure 2. Map of snowfall-weighted 2-m temperature differences (ΔT), and scatter heatmaps of site-specific temperature anomalies (T')
against snowfall rates (SF). Thick black lines indicate the extent of the Antarctic continent (including ice shelves). Thin lines show the 100
m, 1000 m, 2000 m, and 3000 m elevation contours. Black dots show the location of 10 selected locations where the scatter density heatmap
of temperature anomaly to climate normal is shown in each insert (same as Fig. 1, but for a single model cell). Dotted lines represent linear
trends computed for each insert on the $\log_{10}(1+SF)$ scale using snowfall-weighting coefficients (following the regression method described
in Servettaz et al., 2020). Days without snowfall or with extremely low snowfall rates, below 0.05 kg m^{-2} d^{-1}, were excluded from the trend
computation. All trends are significant (p value < 0.01). T' – Temperature anomaly to climate normal; SF – Snowfall.

Figure 3. Seasonal cycles of temperature and snowfall averaged over Antarctica. (**a**) climate normals of temperature ($\bar{T}$) and snowfall-weighted temperature ($\overline{T_w}$). (**b**) monthly snowfall. For both panels we included all model points on the Antarctic continent, including ice shelves. Climate normal temperatures were computed as arithmetic (for $\bar{T}$) or snowfall-weighted (for $\overline{T_w}$) average of the same day of year for all the 1979–2020 period, then smoothed with a 30-days rolling mean (see Sect. 2 Methods).
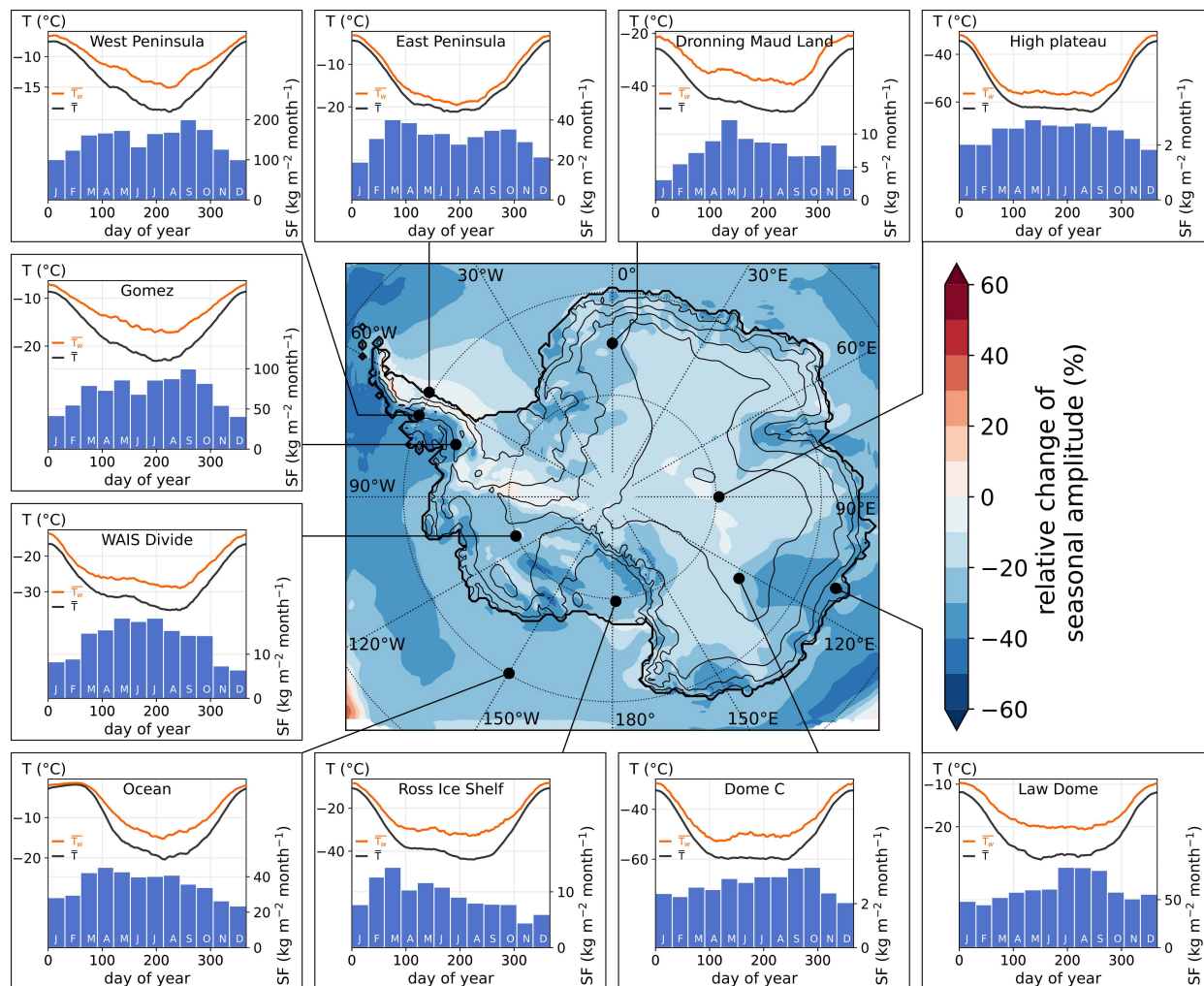
Figure 4. Map of the relative change in seasonal amplitude, defined as the ratio of standard deviations $r_{SD} = \left(\frac{SD(\overline{T_w})}{SD(\overline{T})} - 1 \right) \times 100$ for each model cell, where SD is the standard deviation. Inserts show seasonal cycles of temperature and snowfall for a selection of 10 sites in Antarctica. For each site, climate normals of temperature ($\overline{T}$), snowfall-weighted temperature ($\overline{T_w}$) and monthly snowfall, similarly to Fig. 3. Climate normal temperatures were computed as arithmetic (for $\overline{T}$) or snowfall-weighted (for $\overline{T_w}$) average of the same day of year for all the 1979–2020 period, then smoothed with a 30-days rolling mean.
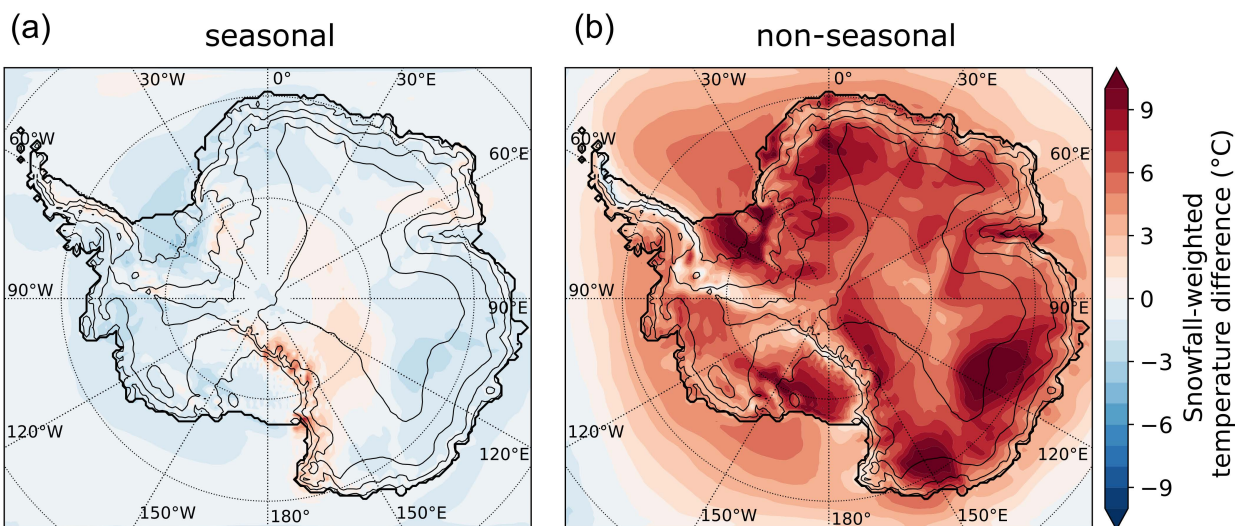
Figure 5. Seasonal and non-seasonal effects of snowfall weighting on temperature difference (ΔT). (a) seasonal effect on temperature difference reflects the temperature changes induced by snowfall seasonality. (b) non-seasonal effects of snowfall weighting, revealing the influence of snowfall event-related warming. The sum of both maps results in the map shown in Fig. 2 (see Sect. 2 methods).


20
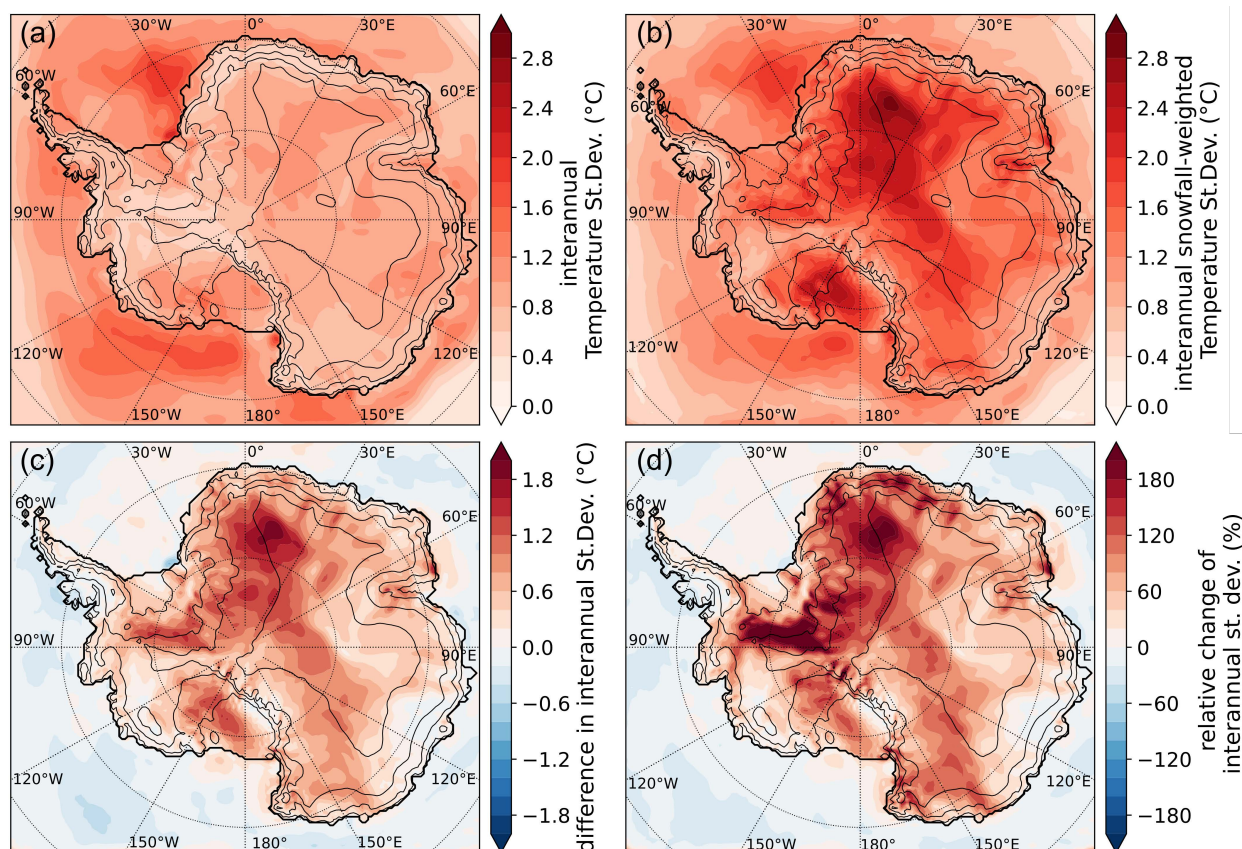
Figure 6. Maps of the change of interannual standard deviation of temperature induced by the snowfall weighting. (**a**) standard deviation of annually averaged temperature $SD(T)$. (**b**) standard deviation of annually snowfall-weighted temperature $SD(T_w)$. (**c**) difference of standard deviations $SD(T_w) - SD(T)$. (**d**) relative change of standard deviation, given by $r_{SD} = \left(\frac{SD(T_w)}{SD(T)} - 1\right) \times 100$. For all definitions, SD is the standard deviation, T_w and T are annual snowfall-weighted temperature and annual temperature average, respectively. Thick black lines indicate the extent of the Antarctic continent (including ice shelves). Thin lines show the 100 m, 1000 m, 2000 m, and 3000 m elevation contours.
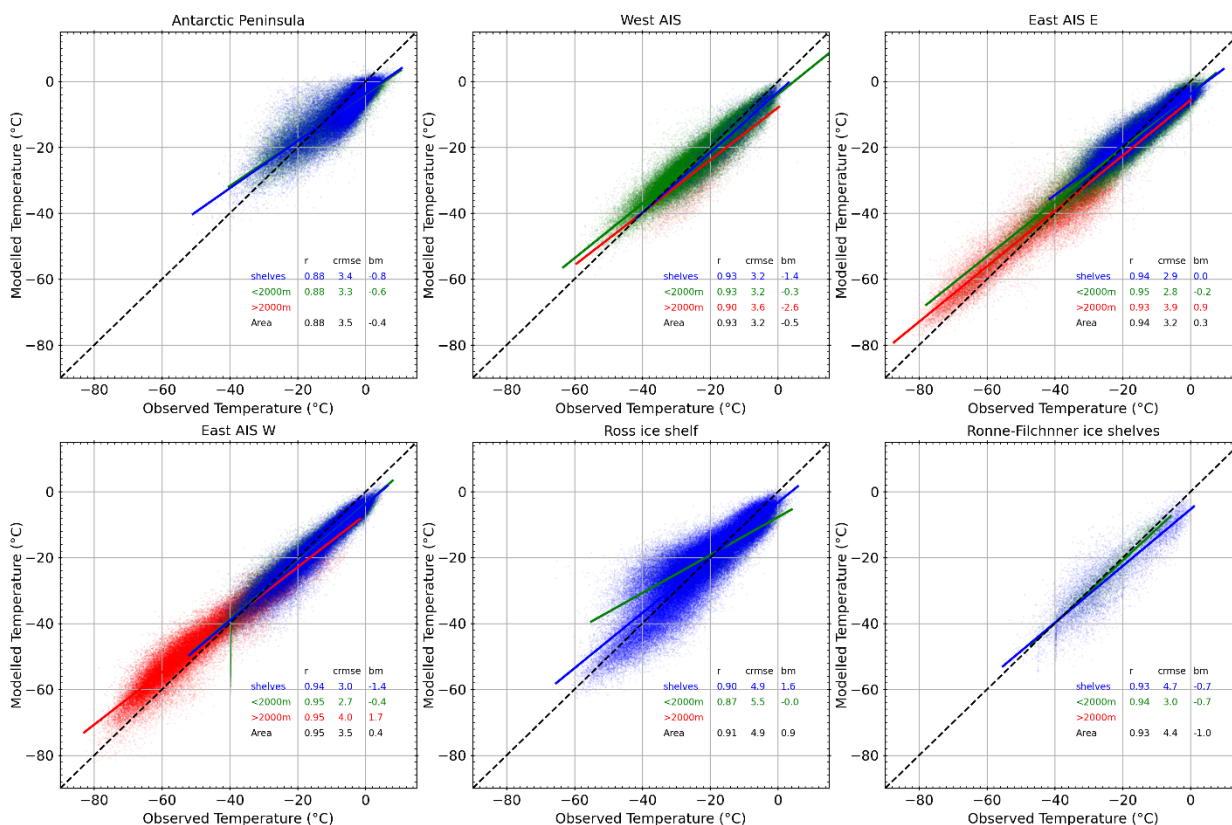
Figure A1. Evaluation of model performance to represent temperature. Scatterplots and linear regressions of modelled (MAR v3.12) vs observed temperature (compilation of automatic weather stations and other measurements Mottram et al., 2021) for different regions (as in Kittel et al., 2021). Slopes slightly lower than 1 indicate that the natural range of temperature variability is greater than what the model can achieve, although the difference is minor. Residual Mean Square Error (RMSE) measures the scattering of modelled temperatures around the observed temperature, and Bias Mean (BM) measures the average difference with the observed temperature. Both give an estimation of imprecision of the model.

21
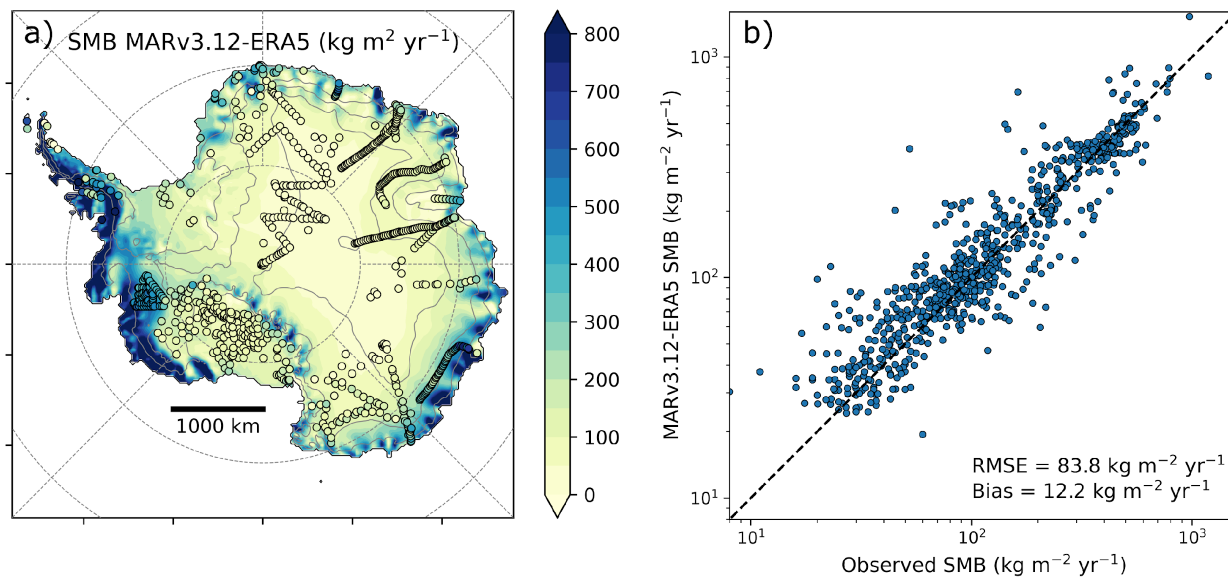
Figure A2. Evaluation of model performance to represent Surface Mass Balance. (**a**) map of Surface Mass Balance (SMB), defined as precipitation minus evaporation and runoff in MARv2.13, compared to accumulation observations (Wang et al., 2016) represented as colour
450   dots. (**b**) log-scale scatterplot of modelled SMB vs accumulation observations. Modelled SMB is higher than observations by a bias of 12.2 kg m^{-2} yr^{-1}.
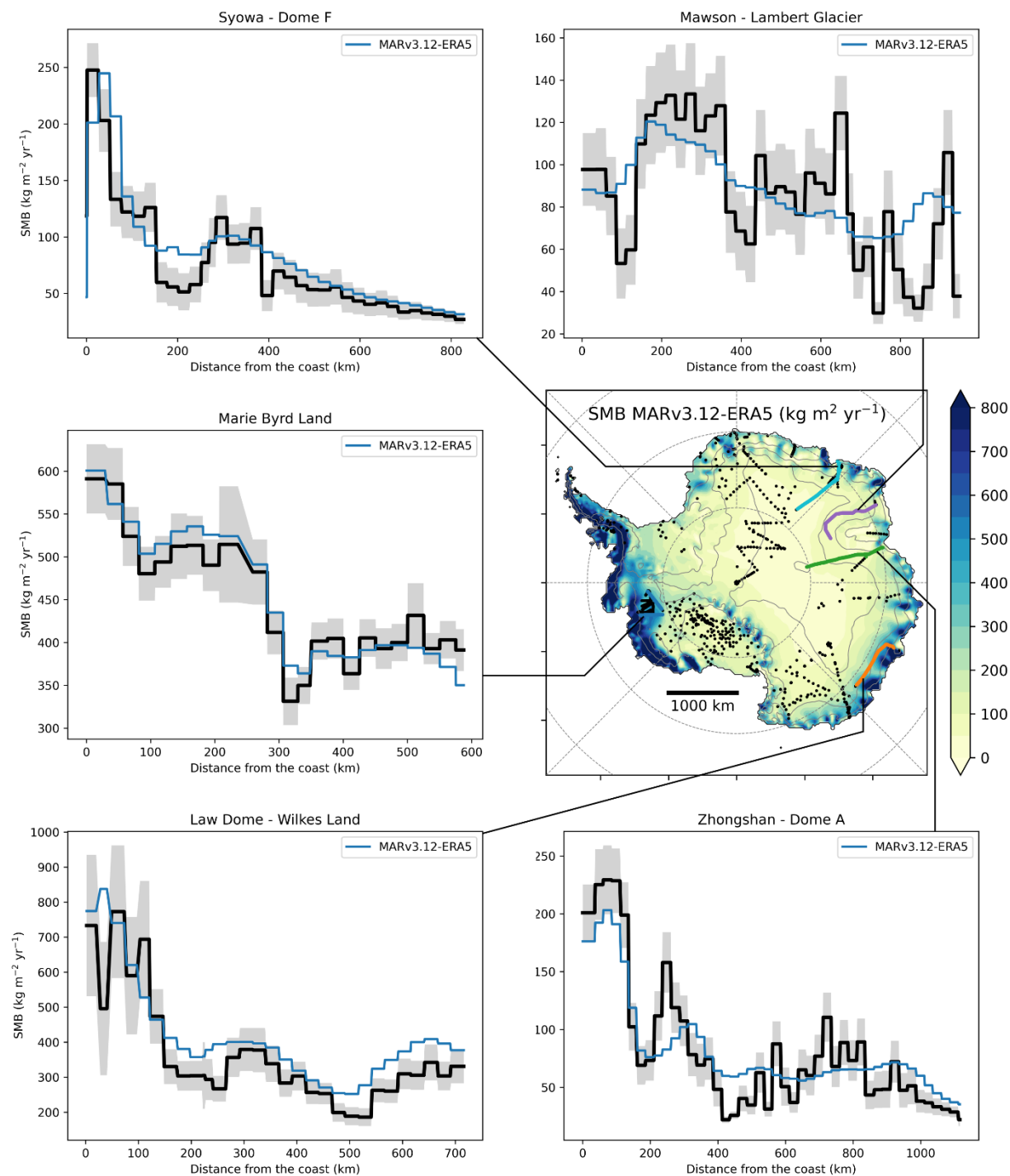
Figure A3. Evaluation of Surface Mass Balance model performance along transects Surface Mass Balance (SMB), defined as precipitation minus evaporation and runoff in MARv2.13 is compared to observations (Wang et al., 2016) along five transects represented by colour lines on the map. MAR tends to slightly overestimate SMB at high elevation sites, and underestimate the variability of small-scale changes. This

could be attributed to unresolved drifting snow transport in MAR due to coarser than real topography (Agosta et al., 2019). Despite these flaws, modelled SMB remarkably follows the observed spatial trends in accumulation.